Reconstruction of Channelized Systems Through a Conditioned Reverse Migration Method

Marion Parquer, Pauline Collon, Guillaume Caumon

Mathematical Geosciences manuscript No.
(will be inserted by the editor)

Reconstruction of Channelized Systems through a Conditioned Reverse Migration Method

Marion N. Parquer · Pauline Collon · Guillaume Caumon

Received: 23 January 2017 / Accepted: 24 July 2017
Published online in Mathematical Geosciences: 21 August 2017
DOI: 10.1007/s11004-017-9700-3

Abstract Geological heterogeneities directly control underground flow. In channelized sedimentary environments, their determination is often underconstrained: it may be possible to observe the most recent channel path and the abandoned meanders on seismic or satellite images, but smaller-scale structures are generally below image resolution. In this paper, reconstruction of channelized systems is proposed with a stochastic inverse simulation reproducing the reverse migration of the system. Maps of the recent trajectories of the Mississippi river were studied to define appropriate relationships between simulation parameters. Measurements of curvature and migration vectors showed (i) no significant correlation between curvature and migration offset and (ii) correlation trends of downstream and lateral migration offsets versus the curvature at half-meander scale. The proposed reverse migration method uses these trends to build possible paleo-trajectories of the river starting from the last stage of the sequence observed on present-day (satellite or seismic) data. As abandoned meanders provide clues about the paleo-locations of the river, they are integrated step by step during the reverse simulation process. We applied the method on satellite images of a fluvial system. Each of the different resulting geometries of the system honors most of the available observations and presents meandering patterns that are similar to the observed ones.

Keywords Stochastic simulation · Fluvial · Turbidite · Oxbow lake · Point bar · Channel evolution · Reservoir

Marion N. Parquer
GeoRessources - UL/CNRS/CREGU
2 rue du Doyen Marcel Roubault. F-54518 VANDOEUVRE-LES-NANCY
E-mail: marion.parquer@gmail.com

Pauline Collon
GeoRessources - UL/CNRS/CREGU
2 rue du Doyen Marcel Roubault. F-54518 VANDOEUVRE-LES-NANCY

Guillaume Caumon
GeoRessources - UL/CNRS/CREGU
2 rue du Doyen Marcel Roubault. F-54518 VANDOEUVRE-LES-NANCY

1 Introduction

Deciphering the fundamental parameters that control the morphology and evolution of meandering systems has been the focus of many researchers for decades (Covault et al., 2016; Jobe et al., 2016; Leopold and Langbein, 1966; Seminara, 2010). These systems can be found in aerial or submarine environments (Leopold and Langbein, 1966; Wynn et al., 2007). In the sedimentary record, channelized systems can also represent interesting reservoirs for natural resources such as water and hydrocarbon (Fitterman et al., 1991; García-Gil et al., 2015; Mayall et al., 2006) or for storage of gas (e.g., carbon sequestration, Issautier et al. 2014).

Turbidite and fluvial systems both migrate in the available space (canyon or floodplain) (Jobe et al., 2016; Wynn et al., 2007). This migration goes along with a perpetual reworking of sediments due to erosion, transport and deposition. Labourdette and Bez (2010) and Peakall et al. (2000) describe a vertical migration (aggradation, Fig. 1a) and two horizontal migrations, one directed downstream, in the direction of flow, and one directed perpendicularly to the flow direction (Fig.1b). The latter is called the lateral migration and contributes to the extension of channel meander loops at small scale and, at a larger scale, to the meander belt. The relative expression of these directions of migration depends on various external and internal factors (e.g., amount of sediment, confinement degree, nature of sediment, paleo-slope, maturity of the system, structural controls) and makes each system unique (McHargue et al., 2011; Wynn et al., 2007).

In addition to gradual migration, the main path of the channel can change abruptly because of avulsions or cut-offs (Hajek and Wolinsky, 2012; Slingerland and Smith, 2004; Stouthamer and Berendsen, 2001). A cut-off occurs when the sinuosity of the channel becomes so high that the channel pinches itself. The trajectory is naturally simplified by the cutting of meander loops. After these disruptive events, paleo-channels and oxbow lakes will be filled with fine-grained material (Issautier et al., 2014; Veeken, 2006). Therefore, paleo-channels can be observed on stratal slices (Miall, 2014; Posamentier and Kolla, 2003). The remnants of oxbow lakes after erosion will provide important clues about paleo-trajectories of the channel. In subsurface studies, well data can also inform about channel facies positions. Thus, the typical subsurface data that are available to constrain the modeling of channelized systems are composed by borehole data, the last channel path and the observable oxbow lakes.

The long-term evolution of the main channel leads to a complex internal architecture of shale and sand deposits. This complexity, mainly due to the perpetual reworking of the sediments, causes heterogeneities at different scales in the final deposit (Jackson and Muggeridge, 2000; Willis and Tang, 2010). For example, various types of point bars are deposited along both sides of the channel and distributed around the meander shape (e.g., counter-point-bars, downstream-migrating fluvial point bars, eddy-accretion deposits) (Ghinassi et al., 2016). Such volumes constitute the main reservoir rocks for fluids hosted in channelized sediments. However, these volumes can be compartmentalized due to the presence of shale drapes deposited on the scour surfaces. Understanding reservoir behavior can be achieved by flow simulation. This implies a good reconstruction of the accretion point bars and of the surrounding objects such as shale drapes.

Many studies have been conducted on the spatial evolution of channels (Peakall et al., 2000; Posamentier and Kolla, 2003; Wynn et al., 2007). Most of them focused

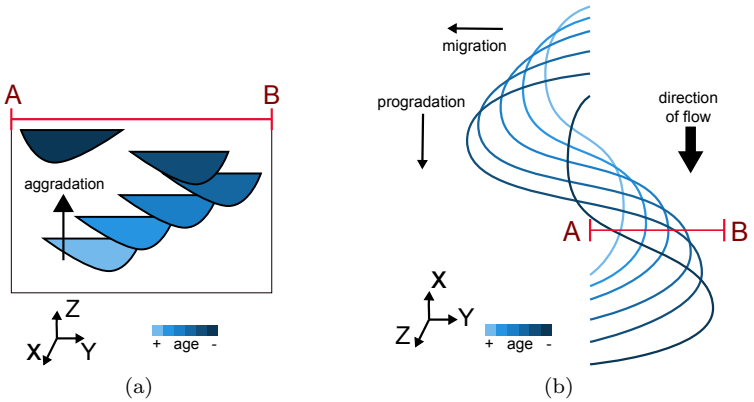

Fig. 1 Channel lateral migration (called migration if perpendicular to flow direction, progradation if in the direction of the flow) and vertical migration (called aggradation): **a** section view, **b** map view

on fluvial systems because they are easily observable and because their day-to-day evolution directly impacts human activities. Thus, forecasting the future evolution of a channel given a geological and hydrodynamic context has been a wide research topic for decades.

Most of the proposed modeling approaches (Edwards and Smith, 2002; Sun et al., 1996) are physical-based methods trying to reproduce the physical processes that generate channelized systems. Many of them are rooted in the seminal works of Ikeda et al. (1981) or Langbein and Leopold (1966) that rely on a hydrodynamic model of the flow inside the channel. This kind of model is calibrated with various parameters such as curvature, channel width values and sedimentary discharge. However, despite the similarity of these forecasts with natural patterns, long-term simulation produces systems that are statistically distinguishable from the natural channels (Howard and Hemberger, 1991). In order to stabilize the long-term behavior of these models, Frascati and Lanzoni (2009) worked on a flow field taking into account other morphological features, such as various morpho-dynamic flow regimes. It has permitted to reproduce the full range of morpho-dynamic regimes which can be found inside a channel of variable meander geometries. Whereas interesting forecasts of channel evolution are given by these methods, their application can be complex and restricted. For example, their parameterization calls for specific types of data such as paleo-hydrodynamic flow and paleo-flow bank erodibility, which are difficult to assess after deposition (Camporeale et al., 2007). Another limit is that these methods give a deterministic solution which does not cover the reservoir architecture uncertainties. To overcome this limit, Lopez (2003) and Pyrcz et al. (2009) introduced stochasticity in their models. Finally, due to the focus on the reproduction of geological processes, data conditioning is difficult, except for well data which can be managed thanks to attraction or repulsion fields.

Descriptive approaches (Deutsch and Tran, 2002; Labourdette et al., 2006; Teles et al., 1998; Viseur, 2004), which focus more on the result of the migration than on the geological processes responsible of the migration, are mainly based on the channel geometry (e.g., curvature, width, depth). This simplified parametric

construction permits to widen the range of applications to poorly known systems in terms of depositional contexts. Although they give good models of channel geometries, they hardly honor seismic and borehole observations in a simple way. In a direct approach, the output model is, indeed, strongly dependent on the hypothesis made on the first channel path. Thus, it can be quite difficult to fit to a precisely observed mature channel shape with a direct evolution model of the channel path.

However, our aim is to reproduce the sedimentary record deposited by the channelized system. Thus, honoring data such as the last channel path is of high importance. Our approach is based on the idea that a good approximation of geological processes should help fitting to all conditioning data by getting closer to the reality. This paper proposes a modeling tool mainly based on the geometric parameters accessible through seismic images such as channel curvature. Starting from the last observed channel path, our algorithm goes back in time reproducing the natural migration of a channel and integrating step by step the oxbow lakes which recorded paleo-trajectories. Although most of the developed approaches only support two dimensions (Howard and Hemberger, 1991; Ikeda et al., 1981; Langbein and Leopold, 1966), the one presented here reproduces the three migration directions of channels, i.e. downstream, lateral and vertical. Our migration model is based on the study of Mississippi maps detailing several trajectories. Thus, the main channel migration steps are reconstructed, opening the way for the reproduction of accretion point bars. In addition to the continuous migration process, the algorithm also aims at reproducing the discrete evolution steps due to brutal events such as meander abandonment. Absolute values of abandonment ages can be given by a few methods such as radiocarbon analysis (Holbrook et al., 2006) or satellite image analysis (e.g., optically stimulated luminescence (Rowland et al., 2005)). Most of the time, on seismic images, only relative abandonment ages can be constrained by the analysis of cross-cuttings and intra point bar erosion surfaces (Durkin et al., 2015).

In order to honor the last channel path observed as conditioning data, some works have been conducted on reverse migration modeling of channelized systems starting from the conditioning data and going back in time. Labourdette (2008) proposed a geometric modeling approach based on the seismic observations of a turbidite system (e.g., final stage, channel belt borders) and on the probable migration of characteristic points of the channel trajectory. The idea of Ruiu et al. (2015) is to reduce the sinuosity of the channel by doing a reverse lateral migration of the channel. The result is a channel that tends to produce a straight line between the initial inflection points. This approach gives interesting stacked geometries for channels which have migrated mainly laterally, but does not reproduce deposits due to potential downstream migration. In the absence of unambiguous subsurface images, Rongier et al. (2017a) simulate the last channel path with a formal grammar method using probability distributions of various geometrical parameters (e.g., meander amplitude, meander wavelength, channel width, channel main orientation). Then, a reverse migration step is generated either with a Sequential Gaussian Simulation (SGS) of migration offset constrained by the curvature of the channel or with a Multiple Point Simulation process. This method reproduces the meandering specificities observed in natural deposits such as lateral and down-system migrations (Posamentier and Kolla, 2003), aggradation (Peakall et al., 2000), diminution of the sinuosity by natural retro-migration of the channel

(Nakajima et al., 2009), abrupt migration (Abreu et al., 2003; Maier et al., 2012), and avulsion (Armitage et al., 2012). However, none of these methods decomposes the migration into the two main directions, lateral and downstream, as advocated for instance by Jobe et al. (2016). Moreover, they do not honor oxbow lakes, which are essential remnants of the evolution of the system.

In this paper, a statistical study of the lateral and downstream migrations of the Mississippi river located in the United States over centuries is proposed (Sect. 2). The aim is to determine how the channel migration could be correlated with morphological parameters. Indeed, the natural migration is the result of the combination of so many internal and external factors that this natural irreversible process is necessarily simplified in the numerical modeling. Then, an inverse modeling method conditioning to oxbow lakes and reproducing the migration patterns as observed in the studied database is presented (Sect. 3) and applied on a satellite image of the Tangnara river located in Russia (Sect. 4). As the available data never sample the channelized system in its whole, the method proposes stochastic realizations. Moreover, the stochasticity helps to assess architectural uncertainties (e.g., location of barriers to flow).

2 Natural Migration of a Channel

2.1 Migration Case Study: Mississippi River

At human time scale, the Mississippi river is a good example of an evolutive meandering channelized system. The US Army Corps of Engineers has dated and mapped the last evolution steps of the river (Fig. 2). This work has been achieved thanks to historic archives for the four youngest paths since 1765 and with aerial photographs for the remnants of older trajectories (Fisk, 1944). Almost twenty stages of migration are observed. This database gives the opportunity to study the link between river geometry and river migration. Most of the previous studies demonstrated a maximum of lateral offset when the ratio of curvature radius to channel width equals three (Furbish, 1988; Hickin and Nanson, 1975; Hooke, 1984). However, channel width can vary locally and is not directly observable on Mississippi maps except for the last channel path of 1944. For the other complete paths, the width should be locally estimated. Otherwise, our aim is to provide a modeling tool also usable on seismic images. On such images, the noise and the limited resolution of these data can make the assessment of river width quite difficult. Thus, we choose not to consider the channel width.

Therefore, we studied the influence of the river curvature on the lateral and downstream migrations by analyzing the four last observed trajectories of the river. Between one thousand and two thousand points were picked along the 1200 km of each trajectory of the channel belt and offsets of migration were computed between pairs of successive channels in terms of evolution through time in the reverse way.

For the study, the channel trajectory is divided into meanders and meanders are divided into half-meanders (Fig. 3). A meander is composed by a pair of opposite loops (Leopold et al., 1964). A half-meander is delimited by inflection points. In order to avoid very small half-meanders, two points at minimum are required between two successive inflection points to define a half-meander. Obviously, the

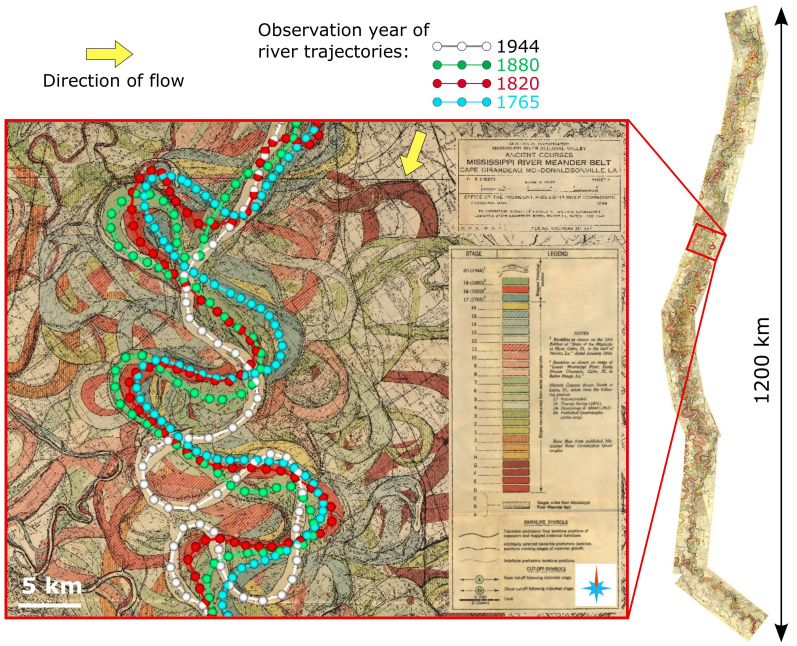

Fig. 2 Picking of the four last trajectories of the Mississippi in 1944 (in white), 1880 (in green), 1820 (in red) and 1765 (in blue) on an extract of map [http://lmvmapping.erdc.usace.army.mil/]

number of points between two inflection points depends of the centerline interpretation. Inside each half-meander, the direction of reverse downstream migration and the direction of reverse lateral migration are defined relatively to the segments connecting the inflection points (dashed grey in Fig. 3). Between two successive channels, the downstream and lateral offsets are given by projecting the points of the younger channel on the older channel along the normal direction to the younger channel path. Then, downstream and lateral offsets are deduced by projection of this vector respectively on the downstream vector and on the lateral vector. The curvature computed on each point p_i of the youngest channel is defined between two consecutive segments as the inverse of the radius of the common circle of the three points defining these two segments.

The global analysis of the results does not demonstrate a clear correlation between the channel curvature and its natural migration offset (Figs. 4a, 4b and 4c). The lateral and the downstream migrations show a majority of migration patterns with downstream and lateral positive offsets (Fig. 4d). The occurrences of patterns with a negative lateral or downstream migration are lower. The same kind of results have been observed on forward migration rates (Appendix A).

2.2 A Curvature-Dependent Migration

The analysis of migration offsets for each half-meander yields more interesting results. Locally, the considered curvature values are the curvature values divided by the maximal observed curvature of each half-meander, hereafter called normalized

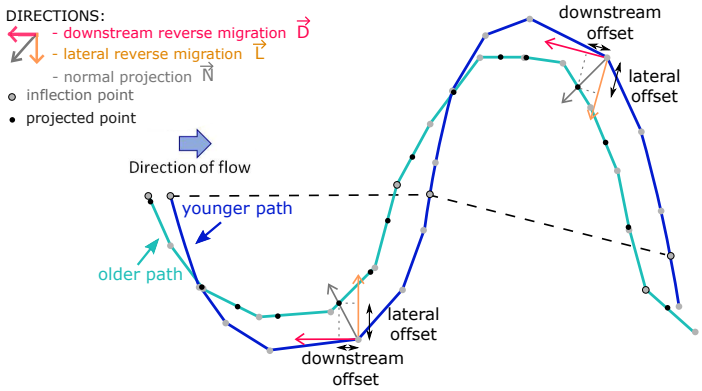

Fig. 3 Points of the youngest channel are projected on the older channel along the normal direction of each point. Lateral and downstream reverse migration offsets are deduced by projection of the normal vector on the lateral or downstream one

curvature. Some of the results are presented in Fig. 5. Inside a half-meander, a light trend can generally be observed between the normalized curvature and the downstream migration offset and between the normalized curvature and the lateral migration offset. Nonetheless, the trends observed are not constant and can be contradictory for two half-meanders of the same river age. In Figs. 5a, 5b and 5f, the downstream migration clearly decreases when normalized curvature increases while the lateral migration follows an opposite trend. The observed correlation is completely inverse in Fig. 5d. It is interesting to point out that the half-meanders of Fig. 5 present various migration patterns (e.g., lateral migration in Figs. 5a and 5f, downstream migration in Fig. 5b and a natural retro-lateral migration in Fig. 5d). The maximal values of lateral and downstream migrations vary with the considered half-meander.

Some half-meanders (Fig. 5c and Fig. 5e) do not present any correlation between the normalized curvature and any of the two horizontal migrations. This is not surprising, considering that the related meanders do not show any visual evidence of correlation. Indeed, the meander of Fig. 5c does not present any significant migration between the two mapped steps. On the contrary, the meander of Fig. 5e has quickly migrated between the two mapped steps and shows the development in the reverse direction of multiple loops in 1820 whereas only one was observed in 1880. Some intermediate steps are missing to understand the link between the normalized curvature and the migration offsets between the two mapped stages. This variety of meander migration speeds has been described in many rivers studies (Brice, 1974).

These results have to be tempered due to the uncertainty on the river mapping in ancient times, the potential influences of the human activities on the river trajectory and of our manual interpretation of the maps. Moreover, the mapped stages are not representative of the gradual migration of the river. It is, however, still interesting to point out that the same results have been observed on forward migration rates (Appendix A).

These plots permit to deduce a model of the half-meander curvature-dependent migration. In the following development, all values obtained by sampling are indi-

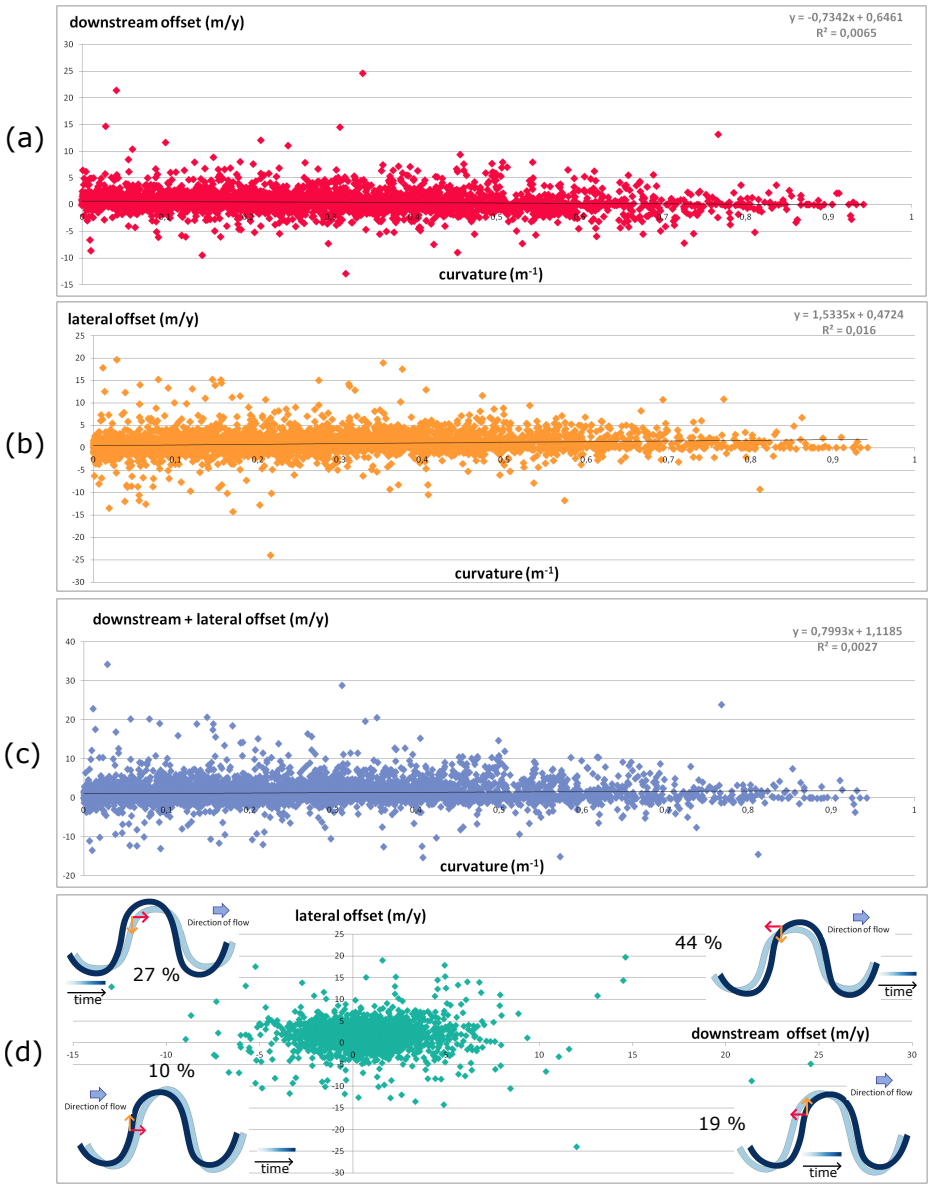

Fig. 4 Horizontal offset versus curvature on four successive paths considered in the reverse direction. **a** curvature versus downstream migration offsets, **b** curvature versus lateral migration offsets, **c** curvature versus sum of the downstream and lateral migration offsets, **d** downstream migration offsets versus lateral migration offsets

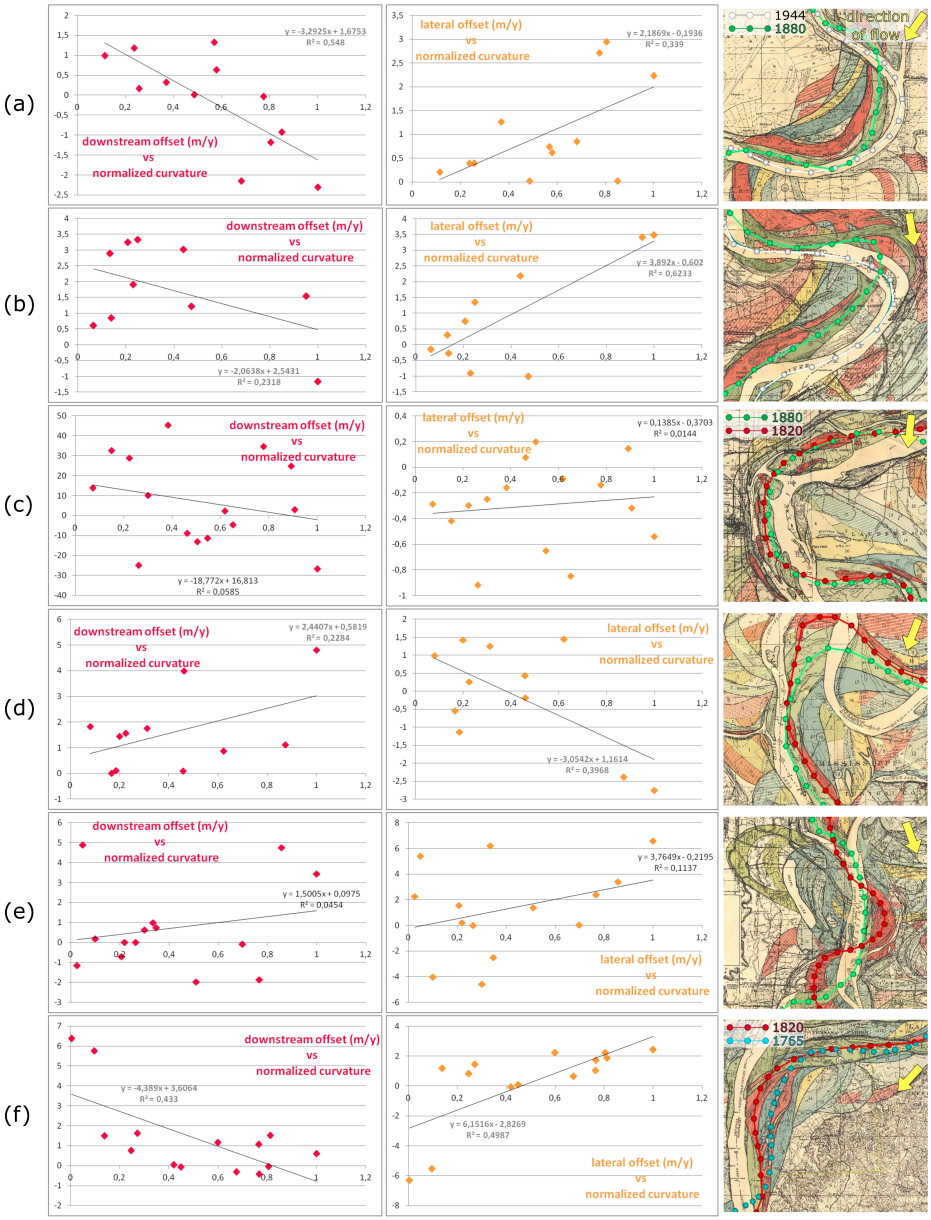

Fig. 5 Plots of offset values (downstream in red, lateral in orange) versus normalized curvature for five meanders of the four last Mississippi trajectories considered in the reverse direction. If some trends can be locally observed, the very low values of some linear correlation coefficients demonstrate the absence of general rules and the high variability of migration patterns

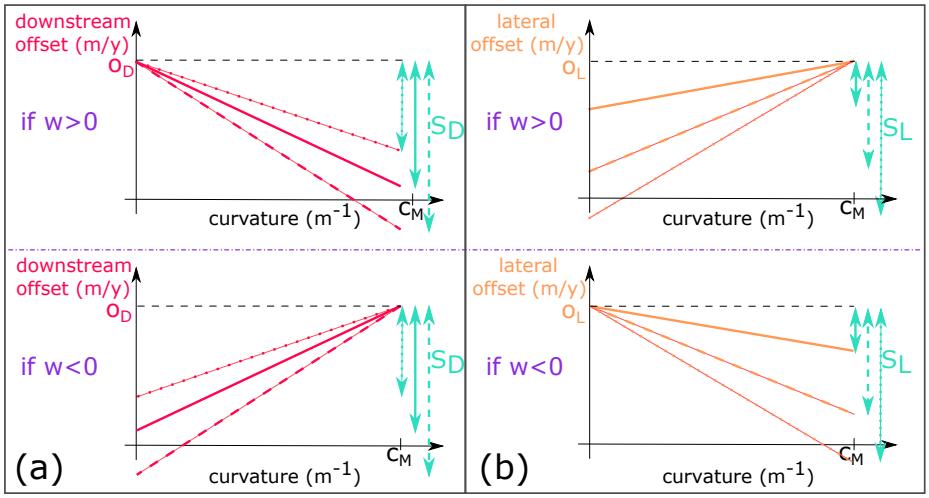

Fig. 6 Schemes of the correlations at the point p_i for three example values of S_L and S_D: **a** between curvature and downstream offset $O_D(p_i)$ for Eq.(1); **b** between curvature and lateral offset $O_L(p_i)$ for Eq.(2)

cated in lowercase and all values deduced from the equations or channelized system analysis are indicated in uppercase. Vectors are indicated in bold.

Because the maximal offset of lateral or downstream migration varies according to the considered half-meander, a sampling of these maximal values o_D and o_L from probability distributions is proposed. A positive or negative weighting by the local curvature is then applied to reproduce the diversity of half-meander behaviors: the curvature weight w is uniformly sampled from the set of discrete values $\{-1; 1\}$. The horizontal offsets of migration are then smoothed according to the local curvature $c(p_i)$ at the point p_i normalized by c_M the local maximal curvature. The smoothing parameters s_D and s_L are sampled from a uniform distribution defined between 0 and two times the maximal offset o_D or o_L.

If w is positive, the reverse downstream migration offset O_D decreases when curvature increases (Fig. 6) as

$$O_D(p_i) = \begin{cases} o_D - s_D \times \frac{c(p_i)}{c_M} & \text{if } w > 0 \\ o_D - s_D \times \left(1 - \frac{c(p_i)}{c_M}\right) & \text{if } w < 0 \end{cases}. \tag{1}$$

Similarly, the reverse lateral migration offset O_L increases when curvature increases (Fig. 6) as

$$O_L(p_i) = \begin{cases} o_L - s_L \times \left(1 - \frac{c(p_i)}{c_M}\right) & \text{if } w > 0 \\ o_L - s_L \times \frac{c(p_i)}{c_M} & \text{if } w < 0 \end{cases}. \tag{2}$$

A negative w value reverses the influence of the curvature (Fig. 6).

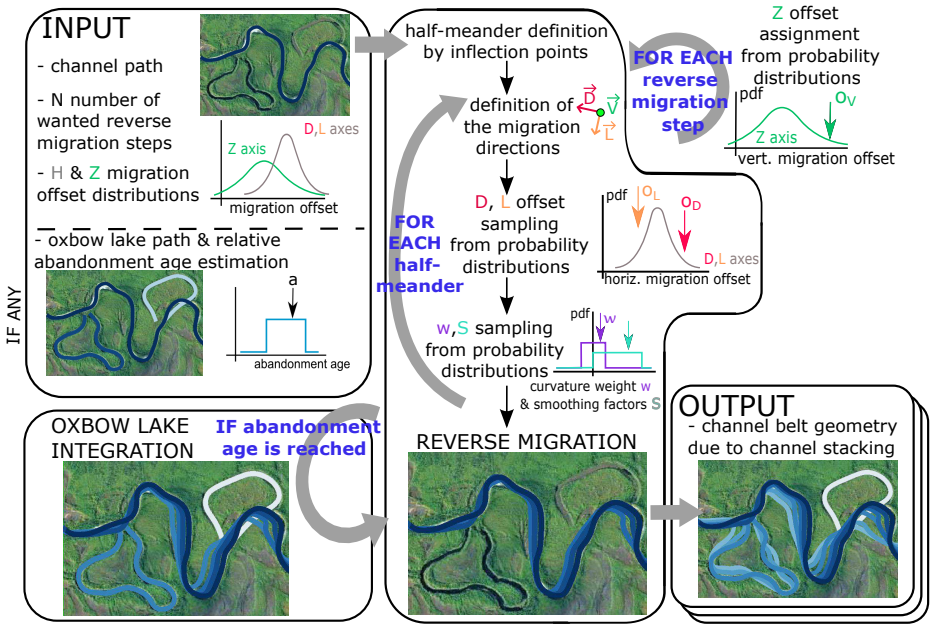

Fig. 7 The reverse migration method accepts data that are available from seismic images such as picking of the main channel path and of its oxbow lakes, estimated minimum and maximum abandonment ages of these abandoned meanders, probabilistic distribution of migration offsets and a number N of migration steps. The outputs correspond to different stochastic three-dimensional architectures of the reservoir. The algorithm is detailed in Appendix B [Google Earth $63°3439.69" N$ $123°3502.08" E$]

3 Reverse Migration Modeling

The study made on the Mississippi system shows the positive or negative influence of the channel curvature on its migration at half-meander scale. This observation can be used as a constraint for migration modeling. A complete reconstruction of channel belts is proposed with a method that only necessitates information that is deducible from seismic horizon slices or satellite images (Fig. 7, Appendix B). These observations include the geometry of the last channel path and, when available, the meander loops abandoned during channel evolution and the age of their abandonment. For practicality, age is considered as discrete time steps and a maximal number of reverse migration steps is used as an ending condition for the algorithm.

3.1 Stochastic Reverse Migration

Curvature-Dependence Modeling. The reverse migration starts from an initial channel path. This trajectory corresponds to the most recent channel position and to the first step of the reverse migration. Inflection points of the channel path permit to identify meanders and half-meanders (Fig. 8). Probability distributions of horizontal and vertical migration offsets are needed to reproduce the variability of

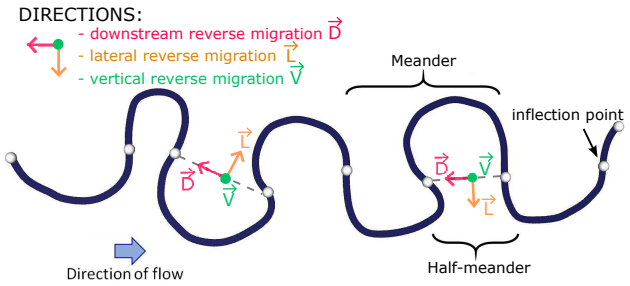

Fig. 8 Definition of the three migration directions at each step thanks to the inflection points of the channel on synthetic data

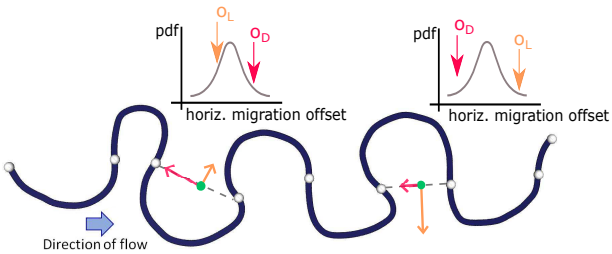

Fig. 9 Sampling of the horizontal and vertical offset migration values in the corresponding probability distributions for each half-meander on synthetic data

migration patterns. In the following examples, Gaussian distributions have been chosen.

Along the channel path, for each half-meander, the downstream and lateral horizontal reverse migration directions (**D** and **L**, respectively) are defined for the current step (Fig. 8). **D** is parallel to the line connecting consecutive inflection points and **L** is perpendicular and oriented toward the center of the meander loop. For each half-meander, a value of maximal horizontal reverse migration offset o_D is sampled from the probability distribution of horizontal offsets (Fig. 9). This value is assigned to the downstream reverse migration **D** and corresponds to the maximal downstream offset of migration in this half-meander for this step. Similarly, another sampling from the horizontal offsets of migration allows to assign the maximal value o_L to the lateral reverse migration L and represents the maximal offset of lateral migration. Values of lateral s_L and downstream s_D curvature smoothing parameters are also sampled from their corresponding distributions and define the minimal offset values. Then, a value of curvature weight w is drawn from the corresponding distribution and applied to the half-meander (Fig. 10). Curvature is computed on each point of the half-meander and local maxima are deduced for each half-meander.

Then, the offset values are computed for each point of the half-meander following the equations deduced from the Mississippi study (Eqs (1) and (2)). The translated points of the half-meander correspond to all points between both inflection points and to the inflection point located the most upstream of the channel path. This ensures the continuity of the reverse migrated channel path at inflection points. At an inflection point p_i, the local curvature $c(p_i)$ is null: depending on

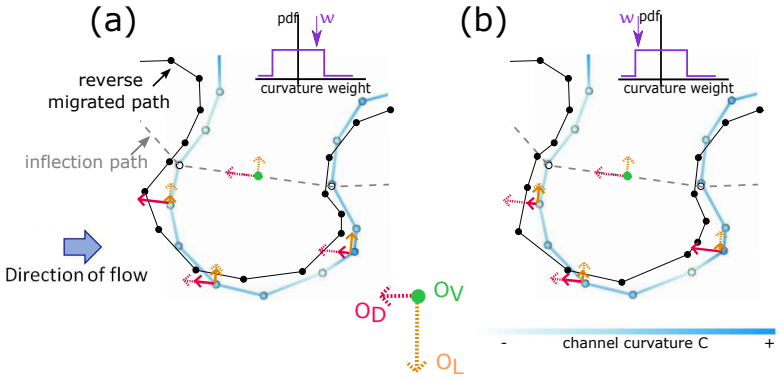

Fig. 10 Influence of the channel curvature on the offset of migration with a sampled value of smoothing equal to o_D in the downstream direction and o_L in the lateral direction on synthetic data. **a** Positive curvature weighting of the horizontal migration, the downstream offset is maximal for lowest curvatures. **b** Negative curvature weighting of the horizontal migration, the lateral offset is maximal for lowest curvatures

the sampled value w, O_L and O_D can be equal to their maximal or minimal value. However, the strict decomposition of the channel path into half-meanders imposes only one translation to each inflection point.

The translated points correspond to the discretization of the channel path centerline. This centerline is wrapped by Non-Uniform Rational B-Splines (Ruiu et al. (2016) and Appendix C) to generate an interpolated volume reproducing the channel shape. Once wrapped, the top surface of the channel is defined by a control mesh made by two external and one central control lines. Furthermore, the offset translation is applied on the control nodes of the NURBS and not on the interpolated shape. This, combined by the strict discretization of the channel path into half-meanders ensures the continuity of the reverse-migrated paths.

As the Mississippi database presents essentially maps, except some cross sections which are too sparse to permit an exhaustive study, the reverse vertical migration has not been studied. Several authors relate the vertical aggradation O_V to be mainly influenced by external factors such as the confinement degree, the sedimentary charge, the accommodation space and, to a lesser point, by morphological parameters such as the sinuosity of the channel (Labourdette and Bez, 2010; Peakall et al., 2000; Wynn et al., 2007). Thus, O_V could be constrained by layer thickness trend or distality if available. When such information is not available, for each step of the sequential reverse migration, the vertical offset value o_V can be sampled at each time step globally for all half-meanders along the channel path from some input probability distribution (Fig. 7) as

$$O_V(\mathbf{p_i}) = o_V \tag{3}$$

and is assigned to all points of the channel path.

Model Discussion. This approach allows to reproduce a wide range of meander migration patterns (Fig. 11). Indeed, the decoupling of the channel horizontal migration in downstream and lateral directions permits to reproduce pure lateral migration (Fig. 11a), pure downstream migration (Fig. 11b) or an intermediate

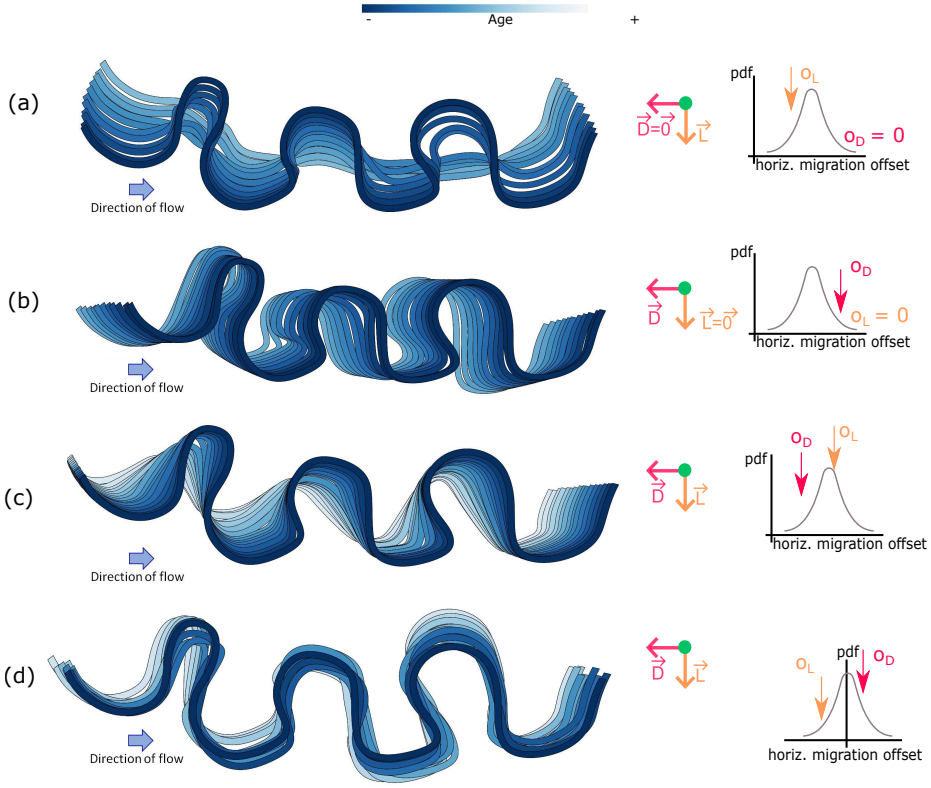

Fig. 11 Variability of the migration patterns applied to synthetic data **a** Pure lateral reverse migration in 10 time steps. **b** Pure reverse downstream migration in 10 time steps. **c** Reverse migration of a channel in 15 time steps. The reconstructed path migrates upstream and becomes less sinuous with the increasing number of steps. **d** Natural reverse migration in 10 time steps with probability distribution accepting negative offsets of lateral and downstream migrations

between both (Fig. 11c). A natural backward migration of meanders can also be simulated when the offset probability distribution includes negative values (Fig. 11d).

The sampling of the horizontal offsets is done at each time step and for each half-meander, in order to reproduce the observed variability of migration offset between two half-meanders for the same age (Fig. 11a). It would be possible to correlate spatially the offsets of migration of the same period if a specific migration rate is known. It would also be possible to correlate the offsets for a specific half-meander if an erosional rate is observed in this specific area.

All these configurations have been observed on the Mississippi maps. In these examples, the reverse migrated channel is located upstream compared to the initial channel when the offset of downstream migration is positive. As the channel reversely migrates, the channel becomes straighter and less sinuous. Indeed, the reverse migration tends to smooth the channel trajectory toward the straight line defined by the inflection points. This diminution of sinuosity is consistent with older channels which are less mature (Brice, 1974).

Between each reverse migration step, the list of inflection points, and so the list of half-meanders, is updated. This permits a complete migration of the system, including inflection points, and a consideration of meander births or extinctions. Working at half-meander scale allows, whatever the sinuosity of the channel, to avoid most of the potential self-intersections all along the reverse process. Indeed, reverse migrating each half-meander independently permits to evolve toward the line connecting two successive inflection points. In this direction, the probability of crossing another meander loop is almost null.

Most of the migration modeling methods (Rongier et al., 2017b; Ruiu et al., 2015; Viseur, 2004) determine the direction of migration along the normal vectors of each point and its offset in a global way. However, the Mississippi river, as many natural channelized systems, presents meanders of various geometries (Brice, 1974). Working between each pair of inflection points allows to reproduce this diversity in terms of channel geometry.

3.2 Conditioning to Paleo-path Indicators

Oxbow Lakes Abandonment Age and Geometry Interpretations. In addition to the last channel path, other channel belt structures can be observed on satellite or seismic images. These objects can be used to constrain the modeling. This corresponds, for example, to oxbow lakes filled by fine particles following their abandonment. For each oxbow lake observed in a meander belt, the absolute abandonment age is difficult to evaluate. Therefore, we use a probability distribution function for relative abandonment ages.

The distance to the middle of the meander belt and the potential erosion by younger oxbow lakes permit to estimate minimal and maximal values of relative abandonment ages. The assigned abandonment age a is sampled from a probability distribution defined between these two extreme values (Fig. 12).

As the natural migration of the channel can erode oxbow lake deposits, the complete geometry of the oxbow lake at the moment of its abandonment may not be preserved in the sedimentary record. An interpretation has then to be performed to extrapolate a probable shape before its integration in the reverse migration algorithm (Fig. 13).

Integration into the Main Channel Path. Each oxbow lake is defined by its centerline (Fig. 14) and wrapped by NURBS (Appendix C) in the same way as the main channel path. When the iterative time step of the algorithm reaches the value of the assigned abandonment age $a - 1$ of an oxbow lake, this oxbow lake is candidate for integration into the main channel path for the next step (Fig. 7). In order to prepare the integration, the algorithm detects the channel closest sections to the oxbow lake extremities (Fig. 14b). Then, the distances between each of the detected channel sections and the oxbow lake extremities are computed in order to check if they are in the authorized range of distances. Such verification is needed to allow the integration of the complete observed oxbow lake geometry. As a rule of thumb, the distance must range between one and three channel widths (Fig. 14c). If the distance control is successful, the two oxbow lake extremities are connected to the detected sections of the main channel path during the next step corresponding to the age a of the oxbow lake abandonment (Fig. 14d). This oxbow

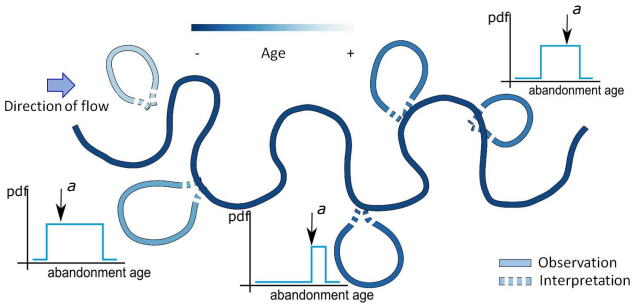

Fig. 12 Abandonment ages a are sampled for each oxbow lake composing the synthetic data inside a discrete probability distribution $U(A_{min}, A_{max})$ with minimal A_{min} and maximal A_{max} deduced from geometric rules. Dashed parts of the oxbow lake traces correspond to interpreted extremities which have been eroded by system migration after abandonment of this oxbow lake

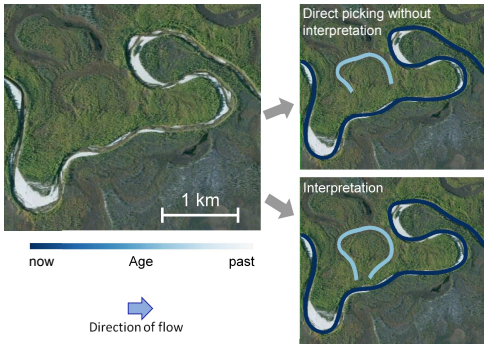

Fig. 13 Interpretation of eroded parts in the trace given in input in order to help a good reconstitution of the paleo-paths [Google Earth $63°1225.33"N$ $122°5953.73"E$]

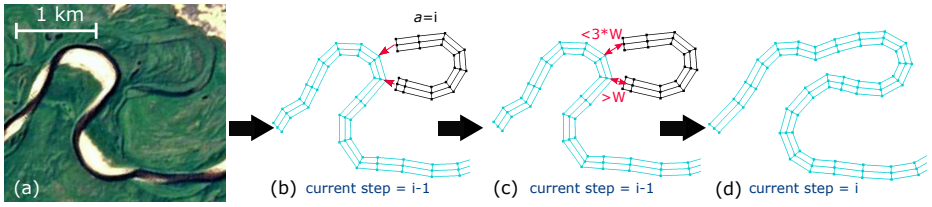

Fig. 14 Reverse modeling of meander cut-off through visualization of the structure of the channel (illustration with the Linde river (Russia)): **a** Satellite image of a river and its oxbow lake. **b** Digitization of the oxbow lake (in black) and of the main channel (in blue) paths. **c** Detection of the channel closest sections and check of the distances. **d** At abandonment age a,the extremities of the considered oxbow lake are projected on the main channel path which is cut between the two projections. The original main channel path is then reconstituted by integration of the oxbow lake path [Google Earth $65°1646.27"N$ $122°2634.65"E$]

lake integration is achieved by connecting the control polygons of both objects. If the distance condition is not respected, the oxbow lake is not integrated. Indeed, for an easy and smooth integration of the oxbow lake, its orientation should fit the channel closest sections orientation. The segment that links its two extremities should be approximately parallel to the main channel path (Fig. 14) whereas

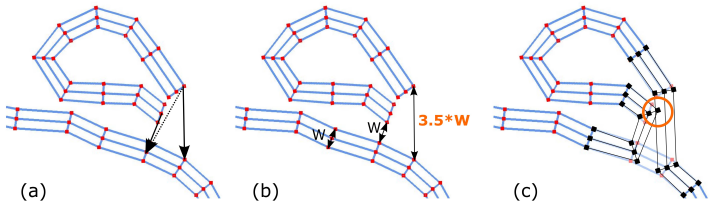

Fig. 15 Example on synthetic data of oxbow lake with perpendicular orientation with the main channel path. Visualization of the control polygons (in blue) of the channel and oxbow lake paths, and of the control points (in red). **a** The research of the closest sections of oxbow lake extremities found the same one, a correction needs to be performed. **b** The distance check fails: maximal accepted distance is equal to three channel widths. **c** Example of integration: if it were authorized, the channel would pinch itself

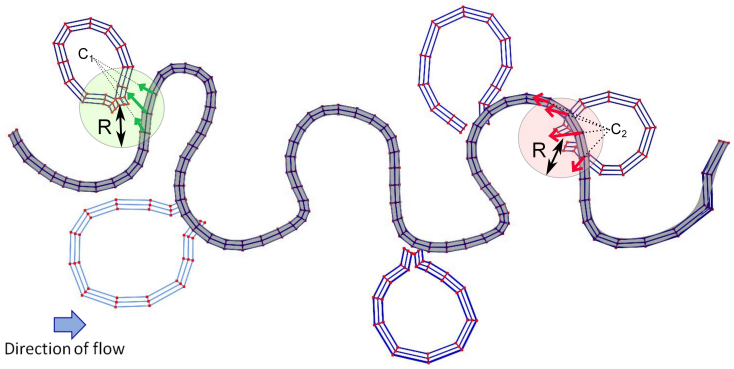

Fig. 16 Attraction and repulsion of oxbow lakes during reverse migration process on synthetic data. Visualization of the control polygons (in blue) of the channel and oxbow lake paths, and of the control points (in red). At abandonment time step, if the oxbow lake is too far from the main channel path (left) the main channel path is attracted towards the center C_1 of the oxbow lake. If the oxbow lake is too close (right) the main channel path is repulsed from the center C_2 of the oxbow lake

the integration will not be possible if these segments are perpendicular (Fig. 15). This direct connection between the extremities of the oxbow lake and the channel justifies the importance of the interpretation of the abandoned meander loop. Naturally, a channel always chooses, indeed, the path of lower energy (Langbein and Leopold, 1966). In the case of a neck cut-off, it corresponds to the cutting of the meander loop when its bends are very close. Thus the interpreted oxbow lake should present a neck made by two extremities that are quite close to each other and are also close to the main channel path at the abandonment age. The following migration of the system may erode the neck due to its proximity to the new channel path. Unsuccessful distance checking for both extremities happens when oxbow lakes are located very far from the main channel or, conversely, in the middle of the channel belt. In the first case, the reverse migration process needs to be attracted by these conditioning data (Fig. 16) which can be located at one border of the channel belt. In the second case, the reverse migration process needs to be repulsed from the area of the considered oxbow lake: until the integration of this abandoned meander, this area must be indeed avoided by the migration process.

Otherwise, reverse migration steps could erode an observed abandoned meander before its integration. Such a realization would suppose that the oxbow lake has been successively abandoned and eroded. In this case, this abandoned meander would not be observable on the image, which is not the case. Thus, attraction or repulsion vectors are defined equal to the current horizontal migration offset and oriented toward the targeted oxbow lake or in the opposite direction of the oxbow lake to avoid (Fig. 16). These repulsion or attraction vectors are applied on restricted areas of the channel path. These zones are defined by a circle centered around the neck of the considered oxbow lake and with a radius R equal to half the mean wavelength of the channel path. The mean wavelength of the channel is defined by the mean distance between two successive inflection points. The offset of attraction or repulsion is weighted by the inverse distance to the center of the oxbow lake (Fig. 16). This prevents brutal distortion of the channel path between sections inside and outside the restriction area.

Finally, if a complex configuration has prevented the integration of an oxbow lake at the wanted step (Fig. 15), the integration is delayed to the next step while conserving the relative age order between oxbow lakes. This postponement to posterior steps calls for adapting the ending condition of the algorithm. In our implementation, the number of reverse migration steps can be increased up to three times the target number of steps in order to improve conditioning rate. This value has been arbitrarily defined after testing various percentages. The best would be to let the algorithm run until all oxbow lakes would be integrated (i.e., without constraint on the maximal number of time steps). However, it is impossible up to now, because all configurations are not handled, and because oxbow lake relative ages may also need to be reconsidered during reverse migration (e.g. Fig. 15). Without such improvements, there is a risk for the algorithm to fall into an infinite loop.

The integrated abandoned meander loops extend the channel reverse migration to the complete meander belt and permit to reproduce the natural reworking of the channel belt (Fig. 17). Conditioning to fairway data is not considered here but could be easily handled. Indeed, fairway datum can be considered in the algorithm as indicator of past meander location in the same way as an oxbow lake. Information about the paleo-orientation of the migration can be observed on fairway data through the stacking patterns of point bars and used to orient the meander loop.

4 Application to a Satellite Image

We tested the reverse migration method on a 15 * 4 km satellite image of the Tangnara river located in Russia (Fig. 18a) [Google Earth $36°12'34.31"N$ $123°00'01.02"E$]. This river presents 24 oxbow lakes that we digitized and classified by relative abandonment ages (Fig. 20). The probability distributions of abandonment ages were attributed by considering the distance to the channel and relative locations of the other oxbow lakes. A target of 10 reverse migration steps was defined and Gaussian distributions were attributed to horizontal and vertical migration offsets, respectively $N(500,100)$ and $N(100,10)$ in meters. We generated one hundred realizations, of which two are presented in Fig. 18b and Fig. 18c. All realizations have the same parameters. Their differences come from the sampling of migration offsets, curvature weights and abandonment ages. A map of the average occur-

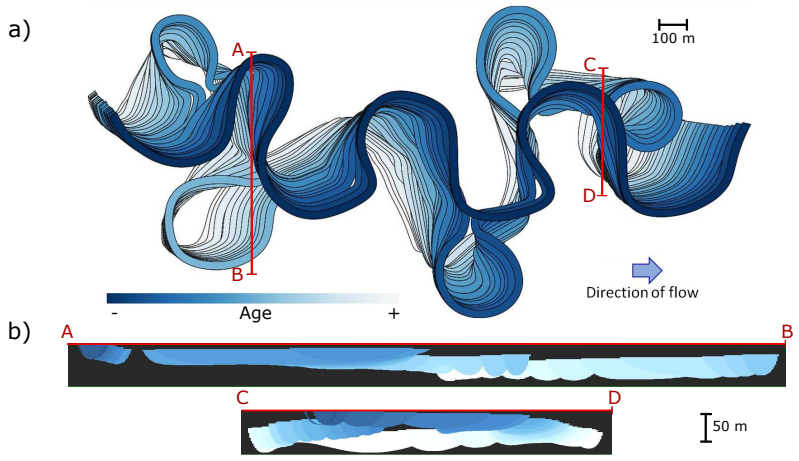

Fig. 17 Reverse migration on synthetic data containing five oxbow lakes. The initial number of reverse migration time steps is set equal to 10. Horizontal offsets follow a normal distribution N(20, 5). **a** Map view. **b** Section views

rences informing about the oxbow lake occurrences of integration and of reverse migration step locations over the hundred realizations is shown in Fig. 18d. It can be noticed that, even with the increased number of reverse migration steps of 300 percents (i.e. maximal 30 reverse migration steps), due to the delayed integration of oxbow lakes after ten steps, some oxbow lakes were not integrated. From one realization to another, the number of successful integrations of oxbow lakes varies between 3 and 15 (Fig. 19a). The same oxbow lakes, for example the 1, 4, 8, 12, 13, 16, 17 and 23 are often let aside. As these are the most ancient oxbow lakes, their successful integration depend on the integration of the youngest abandoned meanders (Figure 20).

The method needs some further developments to accept a wider diversity of oxbow lakes. The improvements concern precise geometrical configurations that are arduous: e.g., when the segment of the oxbow extremities is perpendicular to the main channel path. Another explanation for the non-integration of some oxbow lakes is a mistaken abandonment age estimation. As a perspective, working with scenarios of abandonment ages relying on observed obvious relative abandonment ages could help identifying relative oxbow lakes chronologies that permit reconstruction of more probable paleo-systems. This calls for a better management of relative ages. Relativity between abandonment ages is easy to guess for two juxtaposed oxbow lakes but quite arduous for oxbow lakes far away one from another. Study of the natural clustering of oxbow lakes could help defining relative abandonment ages.

Finally, some oxbow lakes could have been completely eroded by the migration of the system. Indeed, the oxbow lakes that are observable at a given moment do not necessarily retrace the exhaustive history of the channel belt. The simulation of eroded oxbow lakes could help to fit the observed ones and to reproduce the complete channel belt evolution.

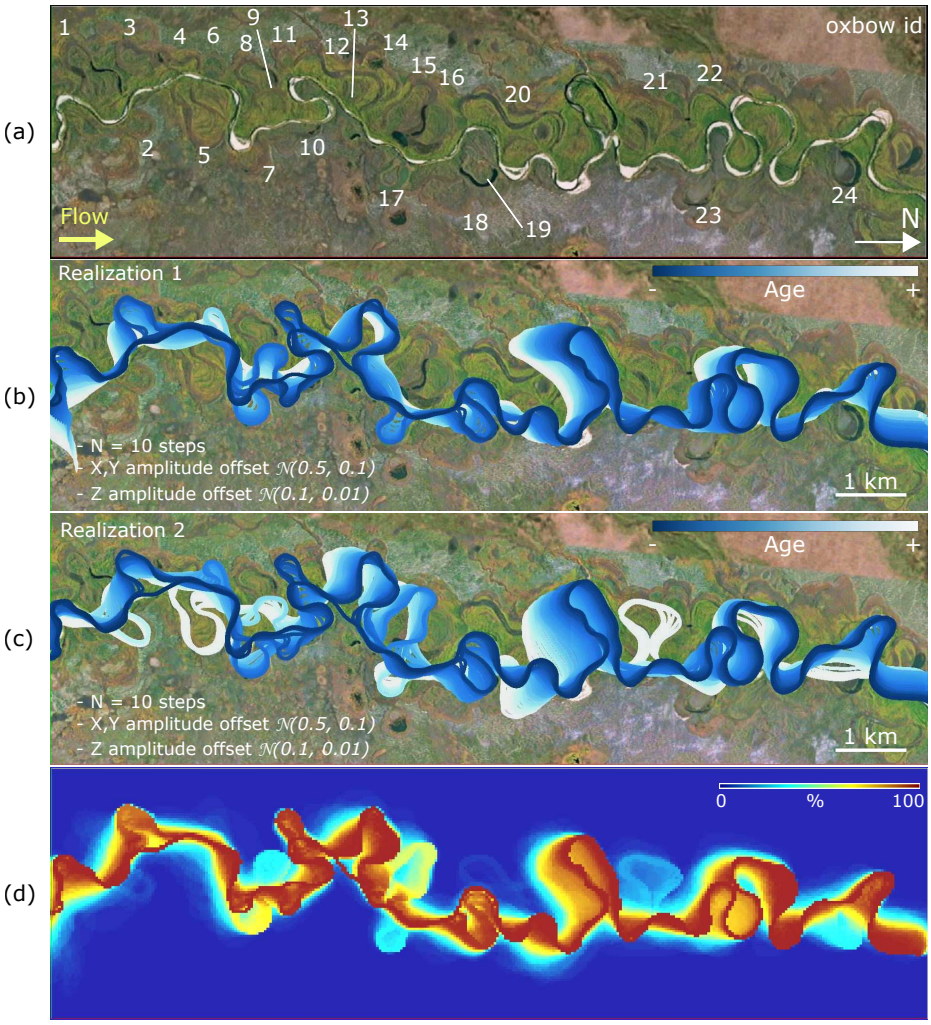

Fig. 18 **a** Satellite image of the Tangnara river (Russia). 24 oxbow lakes can be observed and have been identified by a specific id number. **b**,**c** Realizations of the stochastic reverse migration with conditioning to respectively 9 and 13 oxbow lakes in 30 time steps (the maximal threshold of steps for this application). **e** Map of the average occurrences of 100 realizations [Google Earth $63°09'04.57"N\ 122°59'29.12"E$]

5 Conclusion

Most present-day observations of channel belt systems are suitable to retro-simulate channel evolution and reconstruct possible sedimentary structures and heterogeneities. The types of available datum for channel belt modeling motivate to go back in time to reconstitute the whole system from the last channel position. The lack of information about the paleo-hydrodynamics of the river and of the bank erodibility led us to develop a geometrical-based method of stochastic reverse migration which aims at reproducing the natural geological processes. Moreover, the

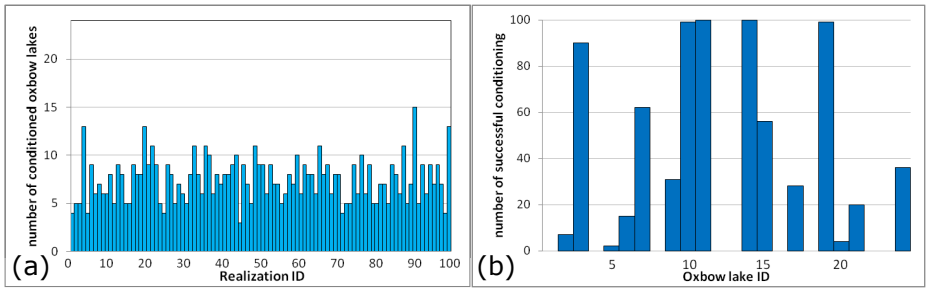

Fig. 19 **a** Number of conditioned oxbow lakes for each realization among the 24 observed paleo-geometries. **b** Number of successful integration for each oxbow lake and for 100 realizations.

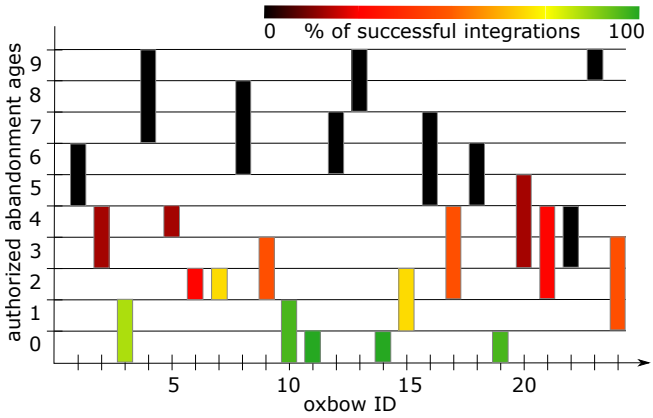

Fig. 20 Probable ages of oxbow lakes versus rate of successful integrations over 100 realizations

complexity and the irreversibility of the natural processes calls for a simplification and a randomization of the model. A statistical study on the Mississippi river suggests an anti-correlation trend of reverse downstream and lateral migration offsets at the half-meander scale. This anti-correlation could maybe be attributed to the energetic compensation between both migration directions of the channel at the half-meander scale. Comparison with correlations observed in other studies about the ratio of curvature radius and channel width could be realized on the last mapped channel path. At this stage, the channel width can be precisely observed. Perfect conditioning to the mapped width could be done using the shape fitting of NURBS objects proposed by Ruiu et al. (2015).

The simulation of the migration in the three directions of the space permits to reproduce many observed patterns of the internal sedimentary architecture in the subsurface. It includes a conditioning to the observable remnants of the system such as oxbow lakes. The stochasticity of the method could help assessing the impact of the heterogeneities and the associated uncertainties on the subsurface flow but calls for appropriate spatial discretization (Botella et al., 2016; Labourdette et al., 2006; Massart et al., 2016). As discussed by Pyrcz et al. (2015), the reverse migration may change statistics on the simulated geometric features of the channel (e.g. wavelength). As channels can naturally show complex variations in time and

space, this can be seen as a strength, even though it raises questions about how to validate the simulation results.

Oxbow lakes with specific orientations are still difficult to integrate and lead to postponing the integration of the older ones. Analysis of their natural clustering could help to assign more accurate abandonment ages and simulation of the eroded ones could facilitate the integration of each oxbow. The development of such a semi-automated tool is one of the short-term perspectives of this work. Another constraint of rotation of the main channel path could be added to overcome this limit and avoid orientation misfit. Finally, the difficulty of the integration of some oxbow lakes can also be due to unexpected behaviors of the natural river which are hard to anticipate in our geometric approach. Oxbow lakes postponed too many times could also result from a wrong age estimation. Their exclusion could be considered. It could also be further used for invalidating some realizations. An a posteriori study of the migration offsets could be done for that purpose.

One of the main perspectives of this work is to test the method on subsurface data of fluvial or turbidite environments. Conditioning to other data than oxbow lakes could also be considered, such as point bars or borehole data. Point bars data can be assimilated to paleo-channel geometries in the same way as oxbow lakes. Well data would indicate sand or shale facies which could be conditioned through the simulation of oxbow lakes geometries inside the channel belt.

Acknowledgements This work was performed in the frame of the RING project at Université de Lorraine (http://ring.georessources.univ-lorraine.fr/). We would like to thank for their support the industrial and academic sponsors of the RING-GOCAD Consortium managed by ASGA. The software corresponding to this paper is available in the GoNURBS plugin of SKUA-Gocad. We also acknowledge Paradigm for the SKUA-Gocad Software and API. The authors thank Michael Pyrcz and an anonymous reviewer for their constructive remarks that helped us to improve this paper.

References

Abreu V, Sullivan M, Pirmez C, Mohrig D (2003) Lateral accretion packages (LAPs): an important reservoir element in deep water sinuous channels. Mar Pet Geol 20(6-8):631–648, doi: 10.1016/j.marpetgeo.2003.08.003

Armitage DA, McHargue T, Fildani A, Graham SA (2012) Postavulsion channel evolution: Niger Delta continental slope. AAPG Bull 96(5):823–843, doi: 10.1306/09131110189

Bézier PE (1983) Unisurf, from styling to tool-shop. Comput Ind 4(2):115–126, doi: 10.1016/0166-3615(83)90017-9

Botella A, Lévy B, Caumon G (2016) Indirect unstructured hex-dominant mesh generation using tetrahedra recombination. Computat Geosci 20(3):437–451, doi: 10.1007/s10596-015-9484-9

Brice JC (1974) Evolution of meander loops. Geol Soc Am Bull 85(4):581–586, doi: 10.1130/0016-7606

Camporeale C, Perona P, Porporato A, Ridolfi L (2007) Hierarchy of models for meandering rivers and related morphodynamic processes. Rev Geophys 45:1–28, doi: 10.1029/2005RG000185.1.

Covault JA, Sylvester Z, Hubbard SM, Jobe ZR, P SR (2016) The stratigraphic record of submarine-channel evolution. Sediment Rec 14(3):4–11, doi: 10.2110/sedred.2016.3

Deutsch CV, Tran TT (2002) FLUVSIM: a program for object-based stochastic modeling of fluvial depositional systems. Comput Geosci 28:525–535, doi: 10.1016/S0098-3004(01)00075-9

Durkin PR, Hubbard SM, Boyd RL, Leckie DA (2015) Stratigraphic expression of intra-point-bar erosion and rotation. J Sediment Res 85(10):1238–1257, doi: 10.2110/jsr.2015.78

Edwards BF, Smith DH (2002) River meandering dynamics. Phys rev E 65(4 Pt 2B):046 303, doi: 10.1103/PhysRevE.65.046303

Fisk HN (1944) Geological investigation of the alluvial valley of the lower Mississippi River. U.S Army Corps of Engineers Mississippi River Commission

Fitterman DV, Menges CM, Al Kamali AM, Jama FE (1991) Electromagnetic mapping of buried paleochannels in eastern Abu Dhabi Emirate, UAE. Geoexploration 27(1-2):111–133, doi: 10.1016/0016-7142(91)90018-8

Frascati A, Lanzoni S (2009) Morphodynamic regime and longterm evolution of meandering rivers. J Geophys Res: Earth Surf 114(F2), doi: 10.1029/2008JF001101

Furbish DJ (1988) River-bend curvature and migration: How are they related? Geology 16(8):752–755, doi: 10.1130/0091-7613(1988)016¡0752:RBCAMH¿2.3.CO;2

García-Gil A, Vázquez-Suñe E, Alcaraz MM, Juan AS, Sánchez-Navarro JÁ, Montlleó M, Rodríguez G, Lao J (2015) GIS-supported mapping of low-temperature geothermal potential taking groundwater flow into account. Renew Ener 77:268–278, doi: 10.1016/j.renene.2014.11.096

Ghinassi M, Ielpi A, Aldinucci M, Fustic M (2016) Downstream-migrating fluvial point bars in the rock record. Sediment Geol 334:66–96, doi: 10.1016/j.sedgeo.2016.01.005

Hajek EA, Wolinsky MA (2012) Simplified process modeling of river avulsion and alluvial architecture: Connecting models and field data. Sediment Geol 257-260:1–30, doi: 10.1016/j.sedgeo.2011.09.005

Hickin EJ, Nanson GC (1975) Lateral migration rates of river bends. J Hydr Eng 110(11):1557–1567, doi: 10.1061/(ASCE)0733-9429

Holbrook J, Autin WJ, Rittenour TM, Marshak S, Goble RJ (2006) Stratigraphic evidence for millennial-scale temporal clustering of earthquakes on a continental-interior fault: Holocene Mississippi River floodplain deposits, New Madrid seismic zone, USA. Tectonophysics 420(3):431–454, doi: 10.1016/j.tecto.2006.04.002

Hooke J (1984) Changes in river meanders: a review of techniques and results of analyses. Phys Geogr 8(4):473–508, doi: 10.1177/030913338400800401

Howard AD, Hemberger AT (1991) Multivariate characterization of meandering. Geomorphology 4:161–186, doi: 10.1016/0169-555X(91)90002-R

Ikeda S, Parker G, Sawai K (1981) Bend theory of river meanders. Part 1. Linear development. J Fluid Mech 112:363, doi: 10.1017/S0022112081000451

Issautier B, Viseur S, Audigane P, Le Nindre YM (2014) Impacts of fluvial reservoir heterogeneity on connectivity: Implications in estimating geological storage capacity for CO2. Int J Greenhouse Gas Control 20:333–349, doi: 10.1016/j.ijggc.2013.11.009

Jackson MD, Muggeridge AH (2000) Effect of discontinuous shales on reservoir performance during horizontal waterflooding. SPE J 5(4):446 – 455, doi: 10.2118/69751-PA

Jobe ZR, Howes NC, Auchter NC (2016) Comparing submarine and fluvial channel kinematics: Implications for stratigraphic architecture. Geology 44(11):G38 158.1, doi: 10.1130/G38158.1

Labourdette R (2008) 'LOSCS' Lateral Offset Stacked Channel Simulations: Towards geometrical modelling of turbidite elementary channels. Basin Res 20(3):431–444, doi: 10.1111/j.1365-2117.2008.00361.x

Labourdette R, Bez M (2010) Element migration in turbidite systems: Random or systematic depositional processes? AAPG Bull 94(3):345–368, doi: 10.1306/09010909035

Labourdette R, Poncet J, Seguin J, Temple F, Hegre J, Irving A (2006) Three-dimensional modelling of stacked turbidite channels in West Africa: impact on dynamic reservoir simulations. Pet Geosci 12(4):335–345, doi: 10.1144/1354-079306-705

Langbein W, Leopold L (1966) River meanders-theory of minimum variance. Physiogr Hydr studies of rivers 15

Leopold LB, Langbein WB (1966) River meanders. Sci Am 214:60–70, doi: 10.1038/scientificamerican0666-60

Leopold LB, Wolman MG, Miller JP (1964) Fluvial processes in geomorphology. Freeman, San Francisco

Lopez S (2003) Modélisation de réservoirs chenalisés méandriformes: approche génétique et stochastique. PhD thesis, Ecole des Mines de Paris

Maier KL, Fildani A, McHargue TR, Paull CK, Graham SA, Caress DW (2012) Punctuated Deep-Water Channel Migration: High-Resolution Subsurface Data from the Lucia Chica Channel System, Offshore California, U.S.A. J Sediment Res 82(1):1–8, doi: 10.2110/jsr.2012.10

Massart BYG, Jackson MD, Hampson GJ, Johnson HD (2016) Effective flow properties heterolithic, cross-bedded tidal sandstones: Part 1. Surface-based modeling. AAPG Bull 100(05):697–721, doi: 10.1306/02011614221

Mayall M, Jones E, Casey M (2006) Turbidite channel reservoirs Key elements in facies prediction and effective development. Mar Pet Geol 23(8):821–841, doi: 10.1016/j.marpetgeo.2006.08.001.

McHargue T, Pyrcz M, Sullivan M, Clark J, Fildani A, Romans B, Covault J, Levy M, Posamentier H, Drinkwater N (2011) Architecture of turbidite channel systems on the continental slope: Patterns and predictions. Mar Pet Geol 28(3):728–743, doi: 10.1016/j.marpetgeo.2010.07.008

Miall AD (2014) Fluvial depositional systems. Springer

Nakajima T, Peakall J, McCaffrey WD, Paton DA, Thompson PJP (2009) Outer-Bank Bars: A New Intra-Channel Architectural Element within Sinuous Submarine Slope Channels. J Sediment Res 79(12):872–886, doi: 10.2110/jsr.2009.094

Peakall J, McCaffrey B, Kneller B (2000) A process model for the evolution, morphology, and architecture of sinuous submarine channels. J Sediment Res 70(3):434–448, doi: 10.1306/2DC4091C-0E47-11D7-8643000102C1865D

Piegl L, Tiller W (1997) The NURBS book. Springer-Verlag, London, UK

Posamentier HW, Kolla V (2003) Seismic geomorphology and stratigraphy of depositional elements in deep-water settings. J Sediment Res 73(3):367–388, doi: 10.1306/111302730367

Pyrcz M, Boisvert J, Deutsch C (2009) ALLUVSIM: A program for event-based stochastic modeling of fluvial depositional systems. Comput Geosci 35(8):1671–1685, doi: 10.1016/j.cageo.2008.09.012

Pyrcz MJ, Sech RP, Covault JA, Willis BJ, Sylvester Z, Sun T (2015) Stratigraphic rule-based reservoir modeling. Bull Can Pet Geology 63(4):287–303, doi: 10.2113/gscpgbull.63.4.287

Rongier G, Collon P, Renard P (2017a) A geostatistical approach to the simulation of stacked channels. Mar Pet Geology doi: 10.1016/j.marpetgeo.2017.01.027

Rongier G, Collon P, Renard P (2017b) Stochastic simulation of channelized sedimentary bodies using a constrained l-system. Comput Geosci doi: 10.1016/j.cageo.2017.05.006

Rowland JC, Lepper K, Dietrich WE, Wilson CJ, Sheldon R (2005) Tie channel sedimentation rates, oxbow formation age and channel migration rate from optically stimulated luminescence (OSL) analysis of floodplain deposits. Earth Surf Proc Land 30(9):1161–1179, doi: 10.1002/esp.1268

Ruiu J, Caumon G, Viseur S (2015) Semiautomatic interpretation of 3D sedimentological structures on geologic images: An object-based approach. Interpretation 3(3):63–74, doi: 10.1190/INT-2015-0004.1

Ruiu J, Caumon G, Viseur S (2016) Modeling Channel Forms and Related Sedimentary Objects Using a Boundary Representation Based on Non-Uniform Rational B-Splines. Math Geosci 48(3):259–284, doi: 10.1007/s11004-015-9629-3

Seminara G (2010) Fluvial sedimentary patterns. Annu Rev Fluid Mech 42:43–66, doi: 10.1146/annurev-fluid-121108-145612

Slingerland R, Smith ND (2004) River avulsions and their deposits. Annu Rev Earth Pl Sc 32(1):257–285, doi: 10.1146/annurev.earth.32.101802.120201

Stouthamer E, Berendsen HJA (2001) Avulsion frequency, avulsion duration, and interavulsion period of Holocene channel belts in the Rhine-Meuse delta, The Netherlands. J Sediment Res 71(4):589–598, doi: 10.1306/112100710589

Sun T, Meakin P, Jossang T, Schwarz K (1996) A simulation model for meandering rivers. Water Resour Res 32(9):2937–2954, doi: 10.1029/96WR00998

Teles V, de Marsily G, Perrier E (1998) A new approach for modelling sediment deposition in an alluvial plain in order to display its heterogeneity. Comptes Rendus de l'Académie des Sciences - Series IIA - Earth and Planetary Science 327(9):597–606, doi: 10.1016/S1251-8050(99)80113-X

Tiller W (1992) Application of knot-removal algorithms for NURBS curves and surfaces. Comput aided design 24(8):445–453, doi: 10.1016/0010-4485(92)90012-Y

Veeken PC (2006) Seismic stratigraphy, basin analysis and reservoir characterisation, vol 37. Elsevier

Viseur S (2004) Caractérisation de réservoirs turbiditiques : simulations stochastiques basées-objet de chenaux méandriformes. Bulletin de la Société Géologique de France 1(75):11–20, doi: 10.2113/175.1.11

Willis BJ, Tang H (2010) Three-dimensional connectivity of point-bar deposits. J Sediment Res 80(5):440–454, doi: 10.2110/jsr.2010.046

Wynn RB, Cronin BT, Peakall J (2007) Sinuous deep-water channels: genesis, geometry and architecture. Mar Pet Geol 24(6-9):341–387, doi: 10.1016/j.marpetgeo.2007.06.001

Appendix A Forward Migration Analysis of the Mississippi River

Migration rates have also been studied on the Mississippi river between pairs of paleo-trajectories in the forward direction of the paleo-flow. The lateral and downstream offsets have been computed in the same way as in the reverse direction but with inversed vectors. The results are close to the ones deduced from the reverse direction: no clear global correlation can be observed between curvature and forward migration. Correlation trends can be observed at the half-meander scale. These smooth correlations vary depending on the considered half-meander.

Appendix B Algorithm of the Reverse Migration Method

The proposed algorithm for channelized system reconstruction requires as input data the number of wanted realizations, the number of targeted reverse steps, the horizontal and vertical distributions of migration offsets, the final channel path centerline, the list of identified oxbow lake centerlines with their corresponding estimated minimal and maximal values of abandonment period. It iterates on the wanted number of stochastic realizations, on the wanted number of the reverse migration time steps and on the number of half-meanders found, to reverse migrate the main channel path while conditioning to paleo-geometries observed. The algorithm 1 is illustrated in Fig. 7.

Appendix C Flexibility in Interactive Channel Modeling brought by Non-Uniform Rational B-Splines

NURBS (Non-Uniform Rational B-Splines) are parametric surfaces defined by a network of control points and an interpolation function (Piegl and Tiller, 1997). The interpolation function is a continuous polynomial function whose degree is directly related to the number of interpolated points (Bézier, 1983). NURBS objects present a curvilinear framework which permits to choose the grid resolution without shape deformation. These surfaces have been combined to define volumetric objects independent from the support by Ruiu et al. (2016). Thus, channel, levees, point bars and lobes can be modeled with NURBS (Fig. 23) allowing to reproduce channelized systems in both fluvial or turbidite contexts.

In many steps of the workflow, the number of control points varies in an inhomogeneous way. It is the case at each connection of two objects (e.g., the integration of an oxbow lake) or at each local deformation of the NURBS object (e.g., the reverse migration process). This decreases the handling of the NURBS object and the computational efficiency (Fig. 24a). Therefore, the algorithm of Tiller (1992) has been implemented to determine the smallest control polygon while minimizing the deformation imposed to the NURBS (Fig. 24b).

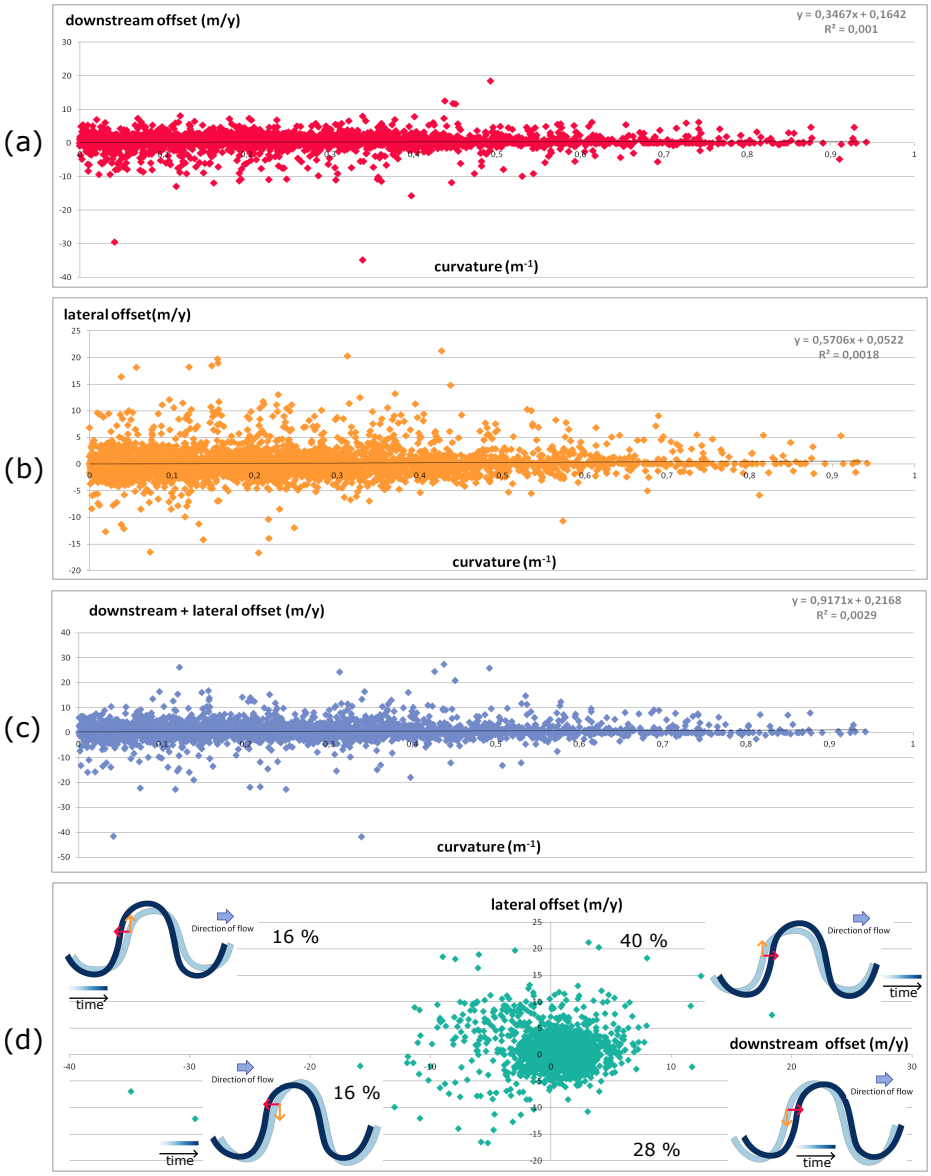

Fig. 21 Horizontal offset values versus curvature on four successive paths considered in the forward direction.**a** curvature versus downstream migration offsets, **b** curvature versus lateral migration offsets, **c** curvature versus sum of the downstream and lateral migration offsets, **d** downstream versus lateral migration offsets

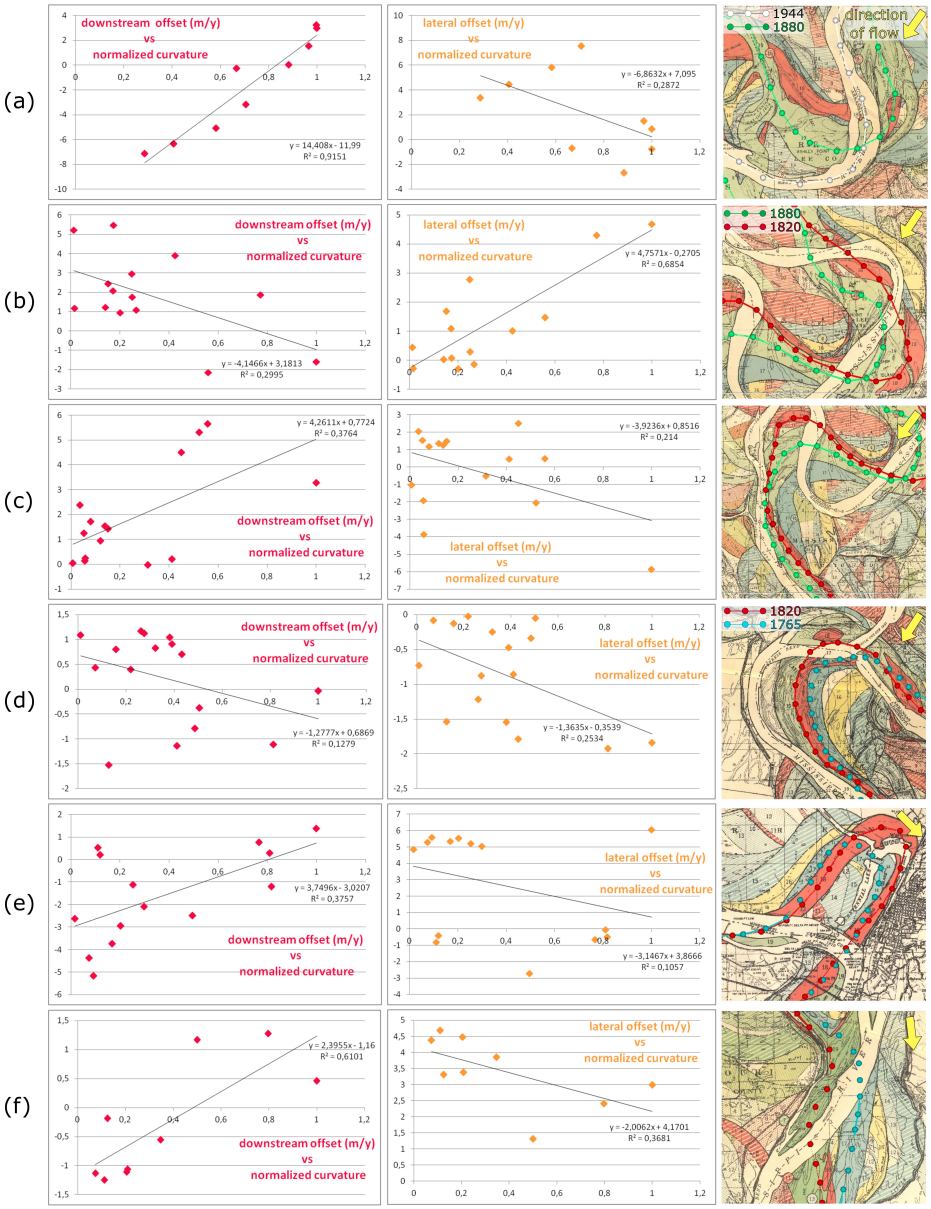

Fig. 22 Plots of values of offset versus normalized curvature for five meanders of the four last Mississippi trajectories considered in the forward direction. They summarize the main trends observed for normalized curvature and downstream migration in red, and normalized curvature and lateral migration in orange. If some trends can be locally observed, the very low values of some correlation coefficients demonstrate the absence of general rules and the high variability of migration patterns

Algorithm 1 Reverse migration simulation workflow

Input: N_r number of realizations wanted, N_s target number of reverse steps, H the horizontal distribution of migration offset, Z the vertical distribution of aggradation offset, the channel path digitization, the list of identified oxbow lake digitizations O_i with corresponding minimal A_{min} and maximal A_{max} values of abandonment period.
Output: N_r different possible geometries of the subsurface

```
for each O_i identified oxbow lake do
    draw the abandonment period a_i between its minimal A_imin and maximal A_imax value
end for
for r_j the current realization id < N_r do
    for s_k the current reverse migration time step < N_s do
        sample the offset of vertical migration inside the probability distribution Z
        detect the inflection points of the current channel path
        define the number N_hm of half-meanders of the current channel path
        for each hm_l of the N_hm half-meanders do
            define the migration directions inside hm_k
            sample the offsets of migration inside the probability distributions H (for the lateral
            and the downstream offsets)
            sample the smoothing values s_L and s_D
            sample the weighting w
            for each point p_m do
                compute the curvature on the current channel path
                smooth the offset depending on smoothing of the half-meander and of the curva-
                ture at the point p_m and of the sampled value w
                translate the point p_m accordingly
            end for
        end for
        if s_k the current reverse migration step == a_i the abandonment period of an oxbow
        lake then
            integrate the corresponding oxbow lake into the current channel path
            if integration of the oxbow lake O_i unsuccessful then
                integration of the oxbow lake O_i postponed to the following time step
                for each O_i that remain to be integrated do
                    a_i = a_i + 1
                end for
            end if
        end if
    end for
end for
return N_r potential geometries of channelized systems
```

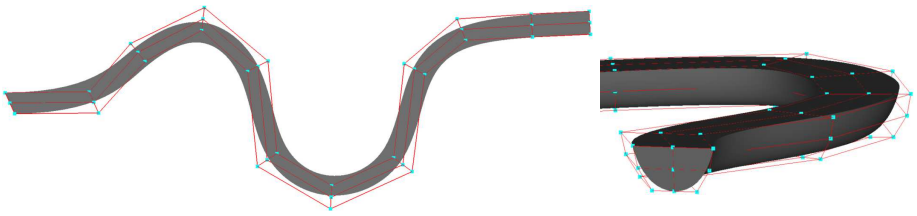

(a) (b)

Fig. 23 Modeling of a channel using 5 NURBS surfaces. Red lines compose the control polygon and the blue points are the control points. **a** Map view **b** Cross view

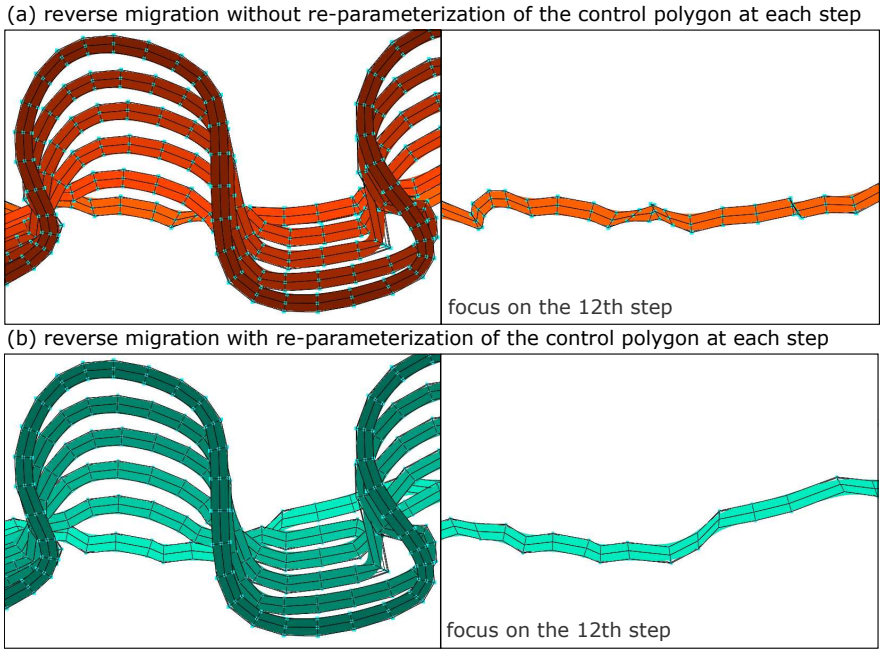

Fig. 24 Re-parameterization during reverse migration process permits to avoid the collapse of sections affecting the channel geometry